International Journal of Thermophysics, Vol. 3, No. 2, 1982

Thermal Conductivity of Oxygen in the Critical Region

L. A. Weber[1]

Received March 19, 1982

The thermal conductivity of oxygen has been measured in a broad region around the critical point by means of Rayleigh light scattering. Measurements were made on two isochores and on the saturation boundary. The results are compared with current methods of predicting the anomalous thermal conductivity in the critical region.

KEY WORDS: coexistence curve; critical point; oxygen; Rayleigh scattering; thermal conductivity; thermal diffusivity.

1. INTRODUCTION

It has long been recognized that the thermal conductivity of a pure fluid undergoes an anomalous increase in the general vicinity of the critical point. In the case of oxygen on the critical isochore, this critical enhancement amounts to about 12% of the total conductivity at a distance of 20° above T_c, and this increases to 90% of the total within a few hundredths of a degree above the critical point. This is generally the same region in which the compressibility becomes very large, and as a result, thermal conductivity measurements by conventional techniques are extremely difficult and subject to large errors. We have therefore made use of Rayleigh light scattering measurements to study the thermal conductivity of oxygen in the critical region. This technique has the advantage that no macroscopic gradients are introduced. In addition, the method is ideally suited for work in this region where the large thermal fluctuations in density scatter light strongly. With the development of the laser and high resolution spectroscopy and other signal processing techniques, it is now possible to measure the properties of scattered light with remarkable accuracy.

[1]Thermophysical Properties Division, National Bureau of Standards, Boulder, Colorado 80303, USA.

0195-928X/82/0600-0117$03.00/0

Along with the development of the experimental techniques, the physics of many-body systems of dense fluids has developed a theoretical picture of the situation which is very useful for interpreting the results. In fact since, in the critical region, the density fluctuations are large compared to the range of intermolecular potentials, the critical enhancement becomes virtually independent of the molecular species; in other words, it exhibits universal behavior, and the results can be calculated with a minimum of data. The theoretical model depends, however, on several approximations and assumptions, and it is the purpose of this experimental work to check the accuracy of some of these approximations in the case of oxygen.

2. CORRELATION OF THERMAL CONDUCTIVITY

Transport coefficients are generally considered as functions of density and temperature. Hanley et al. [1] have correlated the existing thermal conductivity data for oxygen. They constructed excess functions such that the behavior of the thermal conductivity is given by the relation

$$\lambda(\rho, T) = \lambda_0(T) + \lambda'(T)\rho + \Delta\lambda(\rho, T) + \lambda_c(\rho, T) \tag{1}$$

Here λ_0 is the dilute gas value, found from kinetic calculations. The quantity λ' is called the first density correction, and $\Delta\lambda$ is the excess conductivity. The last term, λ_c, is used to describe the critical enhancement. For the details concerning the first three terms on the right side of (1), the reader may consult ref. [1]. Here they will be represented by one term, λ_B, the background thermal conductivity. It is a slowly varying function of T and ρ in the region of interest.

The quantity called the critical excess term has been derived theoretically by Kadanoff and Swift [2] and by Kawasaki [3]. They were able to calculate an expression for the thermal diffusivity in the critical region, which is, approximately,

$$\frac{\lambda_c}{\rho C_p} = \Lambda \frac{k_B T}{6\pi\eta\xi} \tag{2}$$

where k_B is Boltzmann's constant, η is the viscosity, and C_p is the specific heat at constant pressure. The quantity ξ is the correlation length, which will be calculated here according to the expression given by Sengers and Sengers [4],

$$\xi = \xi_0(\Gamma^{-1}\chi_T^*)^{\nu/\gamma} \tag{3}$$

where $\chi_T^*/\rho^{*2} = K_T^*$, the isothermal compressibility, and the * superscript denotes quantities reduced by the critical parameters; Γ and γ are the parameters in the power law expression $\chi_T^* = \Gamma(\Delta T^*)^{-\gamma}$ on the critical isochore, and the reduced temperature and density differences are $\Delta T^* = (T - T_c)/T_c$ and $\Delta\rho^* = (\rho - \rho_c)/\rho_c$. From (3), we see then that on the critical isochore,

$$\xi = \xi_0(\Delta T^*)^{-\nu} \tag{4}$$

where the exponent ν is equal to 0.63. The correlation length amplitude, ξ_0, can be estimated from the method suggested by Basu and Sengers [5]:

$$\xi_0 = R\left(\frac{\Gamma k_B T_c}{B^2 P_c}\right)^{1/3} \tag{5}$$

where R is a universal constant whose value is approximately equal to 0.69. The parameter B is taken from the relationship for the densities on the coexistence boundary,

$$\Delta\rho_{cxc}^* = \pm B|\Delta T^*|^{\beta} \tag{6}$$

and the various exponents are related by

$$\nu = (2\beta + \gamma)/3 \tag{7}$$

Location with respect to the critical point may be designated either by the coordinates $(\Delta T^*, \Delta\rho^*)$ or by (r, θ). Here θ varies from 0 on the critical isochore to ± 1 on the coexistence boundary. In order to calculate the correlation length at densities other than the critical density, Sengers and Sengers [4] generalized (3) to the form

$$\xi = \xi_0 R(\theta)(\Gamma^{-1}\chi_T^*)^{\nu/\gamma} \tag{8}$$

where $R(0) = 1$ and $R(\pm 1) = 1.17$, as calculated from the three-dimensional Ising model and verified experimentally. They suggested that the simplest functional form for $R(\theta)$ should be

$$R(\theta) = 1 + 0.17\theta^2 \tag{9}$$

The shear viscosity, η, also exhibits a weak divergence at the critical point. Like the thermal conductivity, it may be considered to consist of a

background and a critical part. Hanley et al. [1] have also correlated the background viscosity for oxygen. Following Basu and Sengers [6], we will express the viscosity as

$$\begin{aligned} \eta &= \eta_B (q\xi)^{\phi} \qquad \text{for} \quad q\xi \geqslant 1 \\ \eta &= \eta_B \qquad\qquad\quad \text{for} \quad q\xi < 1 \end{aligned} \tag{10}$$

where η_B is the background viscosity. The exponent ϕ is a universal parameter with theoretical values spanning the range $0.054 < \phi < 0.065$, while q depends upon the substance. It has not been determined for oxygen, and we will use here the value determined in ref. [6] for nitrogen, $q^{-1} = 22 \times 10^{-8}$ cm. Since it is raised to a very small power, ϕ, the exact value used makes little difference.

The coefficient Λ in (2) has been calculated by different authors to have values varying between 1.0 and 1.2; see, for example, Burstyn et al. [7]. Measurements on carbon dioxide, steam, and several mixtures have indicated values between 1.15 and 1.2. More recently, however, after very careful measurements, the authors in Ref. [7] arrived at a value of 1.02 ± 0.06. In the comparisons given here, we have used the value 1.2, and any conclusions which we can draw from our results will be discussed in a later section.

Calculation of the correlation length requires a knowledge of the isothermal compressibility. In addition, derivation of the thermal conductivity from the thermal diffusivity requires a value for C_p which also depends on the compressibility. We therefore need a representation for the PVT surface. For oxygen three possibilities exist: a 32-term extended Benedict–Webb–Rubin (BWR) equation [8], a polynomial representation [9], and a nonanalytic scaled equation. Of the three, the scaled equation is by far the best representation in the critical region, and we have used it in its universal form as applied to oxygen. For a complete discussion of this equation, see Section 4.3 of reference [4]. The main drawback of this equation is its limited range. It is only valid for $|\Delta T^*| < 0.025$, $|\Delta \rho^*| < 0.25$. Beyond this region near the critical isochore, the polynomial representation was used, and on the saturation boundary, the BWR equation was used.

Sengers [10] has further pointed out that the range of applicability of (2) is increased if we substitute the quantity $(C_p - C_v)$ in place of C_p. This is a small change since $C_p \gg C_v$ in this region. From the foregoing relations, we see that the thermal diffusivity goes to zero at the critical point approximately as $K_T^{-1/2}$. Since $(C_p - C_v)$ is proportional to K_T to the first power, it follows that $\lambda_c \propto K_T^{1/2}$. The values of the parameters used in the preceding equations are summarized for oxygen in Table I.

Table I. Summary of Parameters Used for Oxygen in Section 2

$T_c = 154.571$ K	$\Gamma = 0.0838$
$\rho_c = 13.63$ mol · liter^{-1}	$B = 1.827$
$p_c = 5.043$ MPa	$\nu = 0.633$
$\Lambda = 1.2$	$\gamma = 1.19$
$\xi_0 = 1.56 \times 10^{-8}$ cm	$\beta = 0.355$
$R = 0.69$	$\phi = 0.057$
$q^{-1} = 22 \times 10^{-8}$ cm	
Relationship between $(\Delta T^*, \Delta\rho^*)$ and (r, θ).	
$\Delta T^* = r(1 - b^2\theta^2)$	$b^2 = 1.3909$
$\Delta\rho^* = r^\beta k\theta$	$k = 1.309$

3. LIGHT SCATTERING

Highly monochromatic laser light incident on a fluid sample is scattered by the spatial variation of the dielectric constant, which in turn is caused by spontaneous fluctuations in the density. These fluctuations also vary with time, causing the scattered signal to be modulated and thus have a frequency distribution. In the case of a simple fluid, the scattered spectrum consists of three Lorentzian shaped lines. The center or Rayleigh line has its maximum at the laser frequency. It is caused by nonpropagating density fluctuations which may also be considered as isobaric entropy fluctuations. The half-width of the Rayleigh line, $\Gamma_R = (\lambda/\rho C_p)k^2$, which is the thermal diffusivity multiplied by the square of the scattering vector, k. The scattering vector is the difference between the wave vectors of the incident and scattered light, $\mathbf{k} = \mathbf{k}_0 - \mathbf{k}_s$; its magnitude is given by

$$|k| = \frac{4\pi n}{\Lambda_0} \sin(\theta/2) \tag{11}$$

where n is the index of refraction of the fluid, Λ_0 is the wavelength of the incident light in vacuum, and θ is the scattering angle. Since the linewidth Γ_R is proportional to the thermal conductivity λ, it may also be considered as consisting of a background and critical part,

$$\Gamma_R = \Gamma_B + \Gamma_c \tag{12}$$

where

$$\Gamma_B = \frac{\lambda_B k^2}{\rho C_p}, \qquad \Gamma_c = \frac{\lambda_c k^2}{\rho C_p} = \Lambda \frac{k_B T k^2}{6\pi\eta\xi} \tag{13}$$

Spontaneous density fluctuations decay according to the laws of hydrodynamics. However, very near the critical point, the correlation range ξ becomes very large, and hydrodynamics must be supplanted by a more general theory. In short, the spectrum becomes k-dependent and Eq. (13) must be modified. We use here the mode-mode coupling theory of Kawasaki [3]. Then Eq. (13) becomes

$$\Gamma_R = \frac{\lambda_B k^2}{\rho C_p}(1 + k^2\xi^2) + \Lambda \frac{k_B T k^2}{6\pi\eta\xi} \frac{K_0(k\xi)}{k^2\xi^2} \tag{14}$$

The first term can generally be calculated from estimations of the background thermal conductivity and C_p derived from PVT data. By the time $k\xi \sim 1$, this term is about a factor of 10 smaller than the second. The function K_0 is

$$K_0(x) = \tfrac{3}{4}\left[1 + x^2 + (x^3 - x^{-1})\arctan(x)\right]$$

with $\lim_{x\to 0} K_0(x) = x^2$, and $\lim_{x\gg 1} K_0(x) = (\frac{3}{8}\pi)x^3$. Thus we see that in the limit $k\xi \gg 1$, the thermal diffusivity becomes independent of ξ (and therefore ΔT^*) for a finite k. The thermodynamic quantities are given by the limiting value at $k = 0$ (forward scattering).

According to Eq. (14), the critical part of the thermal diffusivity approaches an approximately constant value (linear in T) far from critical, whereas $\lambda_c/\rho C_p$ should go to zero. Therefore Hanley et al. [11] have suggested the use of an empirical damping factor, $F(\Delta T^*, \Delta\rho^*)$. This factor has the form

$$F(\Delta T^*, \Delta\rho^*) = \exp\left[-A(\Delta T^*)^2 - B(\Delta\rho^*)^4\right] \tag{15}$$

and they proposed that A and B are universal constants with the values $A = 18.66$ and $B = 4.25$.

Using all of the foregoing relationships, both theoretical and empirical, the expression for the Rayleigh half-linewidth is

$$\Gamma_R = \frac{\lambda_B k^2}{\rho C_p}(1 + k^2\xi^2) + \Lambda \frac{k_B T k^2}{5\pi\eta\xi} \frac{K_0(k\xi)}{k^2\xi^2}\left[1 - \frac{C_v}{C_p}\right] F(\Delta T^*, \Delta\rho^*) \tag{16}$$

In the critical region, the Rayleigh line is too narrow to be measured with the usual types of spectroscopic techniques. It can, however, be measured by correlation techniques. The random density fluctuations,

$\Delta\rho(t) = \rho(t) - \langle\rho\rangle$, are characterized by their time, or autocorrelation function,

$$\langle\Delta\rho(0)\,\Delta\rho(t)\rangle = \langle\Delta\rho^2\rangle e^{-t/\tau_c} \tag{17}$$

which is the Fourier transform of the spectrum. The decay constant τ_c is equal to the reciprocal of the halfwidth of the Rayleigh line, Γ_R^{-1}.

The density fluctuations cause random fluctuations in the intensity of the scattered light. The scattered light is detected by a photomultiplier whose output is fed into an autocorrelator, which builds the correlation function of the photoelectrons. It thus constructs

$$G^{(2)}(\tau) = \langle n(0)n(\tau)\rangle = a^2(1 + e^{-2t/\tau_c}) \tag{18}$$

It allows the direct determination of $\tau_c = \Gamma_R^{-1}$. Thus when Γ_R is very small, the decay time becomes relatively long, and the signal is easily processed by the correlator.

4. EXPERIMENTAL

4.1. Apparatus

This light scattering appartus was originally developed by Ackerson and Straty [12]. The layout of the apparatus is shown in Fig. 1. The beam from an argon ion laser (I in the figure) is directed with mirrors and focused on the center of the sample cell using a long focal length lens. The light scattered at a well-defined angle θ is collimated by the collection optics and focused on the cathode of the photomultiplier. The output of the photomultiplier is fed into a commercially available digital autocorrelator and then into a minicomputer for analysis. If desired, some of the laser beam could be split off and remixed with the scattered light for heterodyne measurements. The sample cell was mounted in the tail of a cryostat and was surrounded by a thin cylindrical copper shield, which was in contact with a liquid nitrogen tank. The shield had three slits which allowed limited optical access to the cell. The sample cell is a heavy wall copper container 6 cm long with quartz windows mounted in the ends. Temperature was controlled with an ac bridge, utilizing a small inexpensive platinum resistance thermometer. A nitrogen gas reflux tube connected the cell with the refrigerant tank for rapid cooling. It was evacuated for measurements in the critical region. Several heaters were wrapped on the cell in a symmetrical manner in order to control the temperature while minimizing thermal

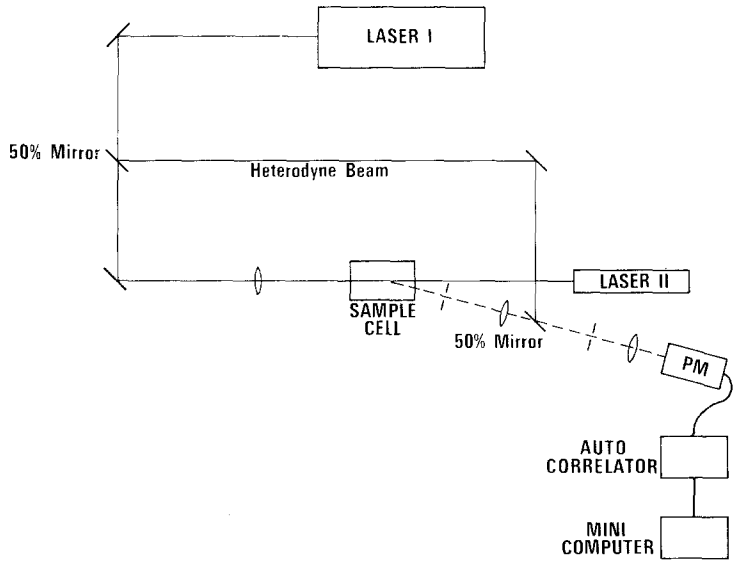

Fig. 1. Schematic layout of the light scattering apparatus.

gradients. Absolute temperatures were measured with a 25 Ω, NBS calibrated platinum thermometer using a 6-dial potentiometer. Temperature control and reproducibility were on the order of 0.5 mK. Laser power was varied from 300 mW far from the critical point to a few milliwatts for the points nearest critical to prevent temperature gradients and convection. The scattering angle was defined by two pinholes and a long focal length lens, and a second lens was used to direct the scattered light onto the photomultiplier. A small 1 mW alignment laser was used to line up the components. The scattered beam path was shielded with several layers of black felt, and measurements were made in a darkened room in order to minimize stray light. The scattering volume had a diameter of less than 0.3 mm, and limiting stops in the collection optics eliminated the window flares at the ends of the cell.

All of the components of the system were mounted on a heavy optical bench, which was levitated by means of air shocks, which in turn rested on several layers of foam padding for the purpose of eliminating extraneous noise from building vibrations. The scattering angle was determined from careful triangulation on the bench top. Most of the data were taken at small angles (8–9°) to observe decay rates which were not too fast to be processed by the autocorrelator. The apparent angle had to be adjusted for the difference between the indices of refraction of the fluid oxygen and

room air, a correction which amounted to about 18% in k^2. Very close to the critical point, the high turbidity and the large density gradient prevented the passage of the incident beam through the 6 cm length of the cell. For measurements in this region, a second laser (II in Fig. 1) was aligned so that its incident beam was in the exact opposite direction from that of the first laser. The collection optics were focused on a point near the rear window of the cell, and measurements were made at the complement of the original angle (171–172°). The total uncertainty due to the scattering angles is estimated at 1% for the forward scattering and about $\frac{1}{2}$% for the backscattering measurements.

Where possible, the homodyne technique was used because it was experimentally easier and the signal to noise ratio was higher. The data were analyzed using Eq. (18). Far from critical, however, the scattered signal is very weak, and some heterodyning from stray flares and reflections in the cell is inevitable, with the result that the correlation function is distorted from the simple single exponential. In this region, it was necessary to mix the heterodyne beam with the scattered light. In this technique, great experimental care must be taken to match the wave fronts so that the two beams will mix efficiently. In the intermediate region, data were measured using both techniques as a check on the results. The two measurements always agreed to within 10%.

The sample density was determined by means of a small flat-plate capacitor mounted on a flange on the bottom of the cell, eliminating the need to measure pressure. The density was calculated via the Clausius–Mossotti relationship given in [13] (ρ in $g \cdot \mathrm{cm}^{-3}$),

$$\frac{\epsilon - 1}{\epsilon + 2} = 0.12361\,\rho + 3.2 \times 10^{-4}\rho^2 - 1.21 \times 10^{-3}\rho^3 \tag{19}$$

The capacitor was located about 3.5 cm below the level of the laser beam. Close to the critical point, the compressibility becomes large enough that adjustment for the variation of the density with height must be made. On the critical isochore within one degree of critical, this correction becomes important. The quantity $d\rho/dh = -\rho^2 K_T$ was calculated using the universal scaled equation of state [4], and the total change in density was found by integrating numerically in height steps of 1 mm. In principle, this adjustment should be fairly accurate. However, in cases where the result could be checked, such as measurements on the saturation boundary, there was a discrepancy between the adjusted densities and the saturation densities calculated from [9]. The discrepancy could be reduced by assuming the existence of a small temperature gradient across the cell, with the top (thermometer) side being warmer and the bottom (capacitor) side colder. In

practice the calculated saturation densities from [9] were used. On the critical isochore, very near T_c, care was taken to make measurements at exactly ρ_c. This was accomplished by moving the focusing lens so that the incident beam was scanned up and down through the cell. Measurements were made at height increments of 1 mm, and the point where the Rayleigh linewidths was a minimum was taken as the point of maximum compressibility and therefore the critical density.

The autocorrelator forms the correlation function of the density fluctuations according to Eq. (18). Delay times varied from 125 μs near critical down to 2 μs. These correspond to Rayleigh linewidths varying from 1 kHz to 64 kHz. The corresponding sampling times varied from about 1 min to about 30 min for the weak signals far from critical. In addition to the 24 data accumulation channels, there were four special channels used to determine the background signal necessary to normalize G.[2] As an additional safeguard, the delay time, τ, was set so that the 24 channels of the correlator spanned six "decades" of the fluctuation decay constant, τ_c. Thus in Eq. (18), $t = 24\tau = 6(\tau_c/2)$. Then since $(1/\epsilon)^6 = 0.0025$, the last four data channels should give the background to within 0.25%. The two methods for calculating the background were compared and generally agreed to within 0.3%. This agreement assured us that we were dealing with a single exponential decay and also that total uncertainty due to the statistical counting process was no greater than about 1%.

In an earlier work [14], we had determined the critical temperature of oxygen to be 154.581 K on the T_{68} temperature scale. However, when studying the power law behavior of thermophysical properties, it is generally desirable to redetermine the critical temperature in the apparatus in which the measurements are made. Small differences in thermometry or small thermal gradients in the apparatus are then cancelled out. In this case the temperature was varied in very small increments over a period of several days, alternately warming and cooling, in an attempt to see the meniscus disappear. Due to the turbidity and vanishing surface tension, this proved to be a very difficult task, with a resulting uncertainty of 0.01–0.02 K. The problem was solved by placing a low power spotting scope in line with the collection optics and observing the laser beam as it passed through the sample. The beam height was adjusted to be just above the meniscus and the sample was heated slightly above critical. In the single phase region the beam is refracted downward by the density gradient. When the sample was cooled into the two-phase region, there was an additional reflected component of the beam. In this way the temperature of the disappearance of the meniscus could be determined with a precision of about 1 mK. With this apparatus, the thermometer indicated a critical temperature of 154.571 K, and all ΔTs given here are relative to this value of T_c.

The oxygen samples came from cylinders of ultra high purity gas, with a total impurity content of 100 ppm or less. The gas was passed first through a trap with a molecular sieve to remove water and then through a paper filter with a pore size of 0.025 μm to remove solid particles, which scatter light very strongly.

4.2. Results

A total of 46 measurements were made on or near the critical isochore, 39 by forward scattering and 7 by backscattering. Values of ΔT ranged from 0.014 to 19.354 K. Nineteen measurements were taken on the saturated vapor and two for the saturated liquid at ΔT varying from -0.002 to -1.7 K. Eleven measurements were also made on an isochore with a density of 15.3 mol · liter^{-1}. The forward scattering data, using the argon ion laser ($\Lambda_0 = 0.5145$ μm), had a value of 2.15×10^4 cm^{-1} for k, while for the backscattering data ($\Lambda_0 = 0.6328$ μm) k had a value of 2.15×10^5 cm^{-1}. The various data points had slightly differing k values due to small adjustments made to the apparatus from time to time. The value of the

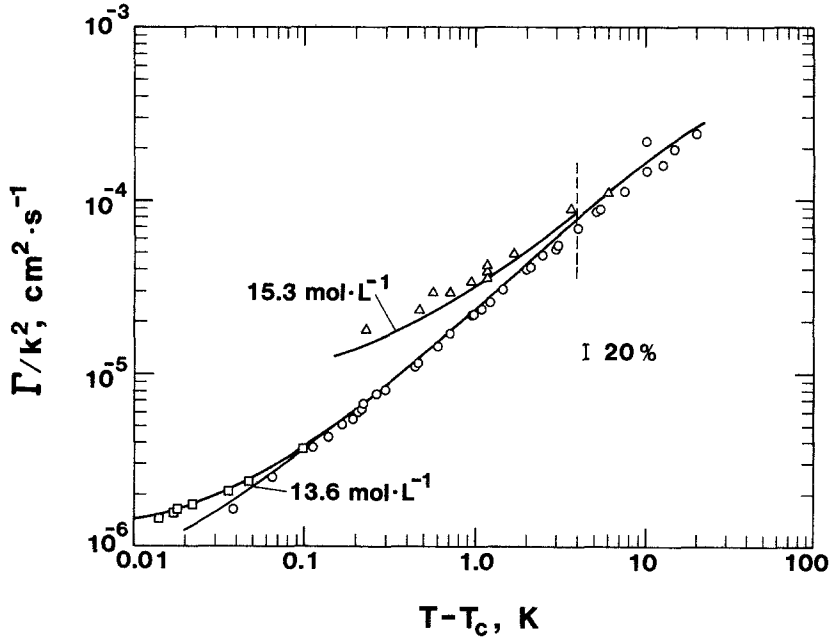

Fig. 2. Thermal diffusivity results on the critical isochore and one near-critical isochore; ○, △, forward scattering; □, backscattering. The curves are from Sengers' calculation using the universal scaled equation of state; dashed line, limit of applicability.

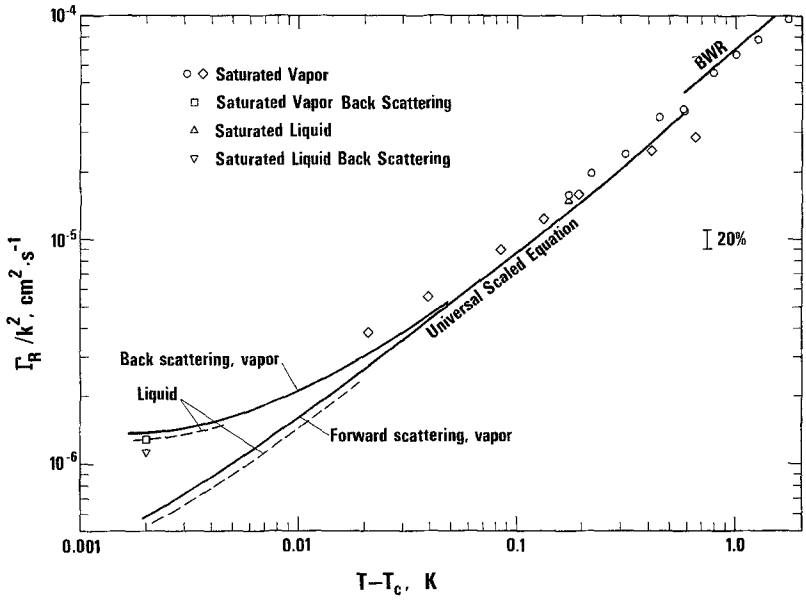

Fig. 3. Experimental results for the saturated liquid and vapor.

index of refraction, n, for oxygen at the critical point was taken from [13] to be 1.084, and it is constant to within about 2.5% in our experimental range. The value of ρ_c used here was taken from [14] and is 13.63 mol · liter^{-1}. The results for the single phase and saturation data are shown in Figs. 2 and 3, respectively, along with values calculated from Eq. (16). Close to the critical point it is seen that the backscattered data deviate from the forward scattered data, illustrating the k dependence when $k\xi \sim 1$. The numerical results are given in Table II.

5. COMPARISON OF EXPERIMENTAL AND CALCULATED RESULTS

In the region studied here, the critical enhancement term in Eq. (16) leads to thermal conductivities which vary in magnitude from a small perturbation on the background thermal conductivity to peaks which rise to nearly 20 times the value of the background conductivity. The estimated uncertainty of the experimental measurements is expected to be 5–10%. With these considerations in mind, it is felt that the experimental and calculated results are in reasonably good agreement. In Fig. 2 we see that

Table II. Thermal Conductivity of Oxygen from Light Scattering Measurements

T (K)	V ($cm^3 \cdot mol^{-1}$)	Thermal conductivity (exp.) ($mW \cdot K^{-1} \cdot m^{-1}$)	T (K)	V ($cm^3 \cdot mol^{-1}$)	Thermal conductivity (exp.) ($mW \cdot K^{-1} \cdot m^{-1}$)
154.569	77.07	770.00	154.791	74.39	162.70
154.550	79.96	282.50	154.831	74.30	156.70
154.532	81.54	215.20	154.862	74.47	142.60
154.487	84.27	152.40	155.015	74.23	121.20
154.439	86.40	125.60	159.573	74.13	54.10
154.400	87.85	120.60	159.880	74.38	52.50
154.378	88.59	105.80			
154.351	89.45	113.40	155.024	73.91	123.00
154.257	92.08	90.60	155.261	73.75	110.00
154.159	94.45	68.70	155.514	73.85	99.00
154.121	95.29	87.00	155.536	73.69	97.00
153.997	97.85	72.30	155.759	73.68	89.10
153.990	97.99	70.70	155.993	73.66	85.50
153.782	101.78	56.50	156.499	73.64	78.30
153.564	105.34	51.70	156.990	73.63	73.10
153.328	108.88	47.60	157.458	73.63	64.30
152.850	115.41	40.50	159.873	73.63	53.70
152.832	115.65	45.70	159.868	74.06	52.70
154.609	76.18	250.70	154.585	73.37	560.00
155.163	75.86	104.30	154.588	73.37	518.00
155.639	75.80	87.50	154.589	73.37	523.00
155.641	75.74	87.10	154.593	73.37	472.00
156.632	75.83	71.50	154.607	73.37	355.00
157.570	75.85	62.70	154.618	73.37	317.00
158.509	75.79	55.60	154.668	73.37	225.00
161.837	76.08	48.00			
164.416	75.35	48.20	154.798	65.46	129.50
164.416	75.35	47.00	155.036	65.39	111.00
164.416	75.35	44.40	155.133	65.39	121.30
166.786	76.46	41.50	155.270	65.36	102.90
168.936	75.72	44.00	155.504	65.34	95.00
173.925	76.71	41.40	155.727	65.39	84.40
			155.730	65.35	97.80
154.707	75.03	184.20	155.742	65.34	92.20
154.736	74.80	175.80	156.211	65.31	85.10
154.761	74.65	167.40	158.123	65.38	69.30
154.777	74.75	160.10	160.483	65.38	55.00
154.785	74.66	157.80			
154.635	74.51	261.00	154.569	70.00	658.00
154.680	74.39	210.90	154.399	62.88	126.50

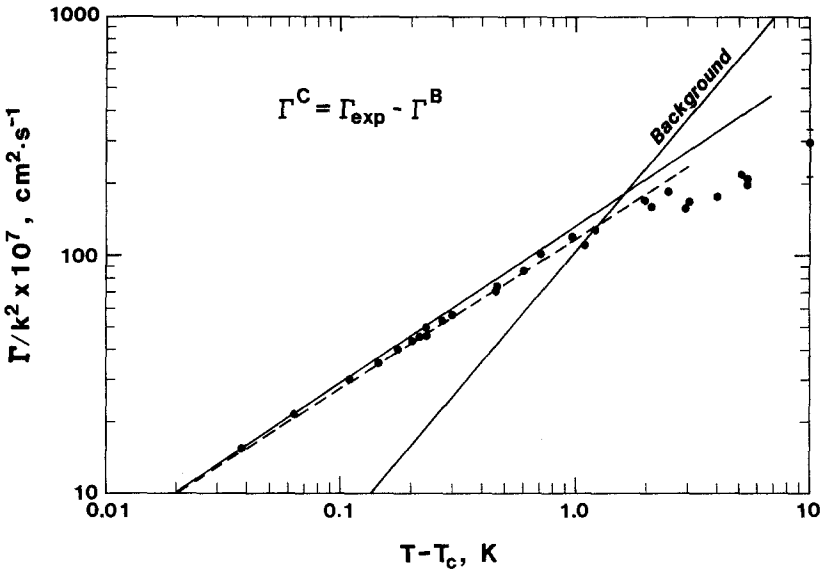

Fig. 4. Variation of the critical part of the thermal diffusivity on the critical isochore; background part also plotted. Solid line, Sengers's model; dashed line, through data.

on the critical isochore, the agreement is very good close to T_c, and that the k dependence of the backscatter data is quite well represented. It is worthwhile to consider some of the individual parameters in Eq. (16) and the effect which their uncertainties would have on the results.

When the results on the critical isochore were first considered, it was found that the good agreement near T_c deteriorated rapidly to about 20% disagreement near the limit of usefulness of the scaled equation of state ($\Delta T = 3.9$ K). The nature of this departure is better seen in Fig. 4, where the calculated background term has been subtracted from the experimental data. In the figure it is seen that although the critical term data follow a power law behavior, they do show a systematic departure from the calculated line. This power law apparently breaks down, and the deviations become large at about $\Delta T = 2$ K. Also shown is the magnitude of the background term, and it can be seen that the agreement becomes poor in just the region where this term begins to dominate. From this we conclude that there is a systematic error in the background values used in the calculations. Modifying the background thermal conductivity by 17–18% would allow good agreement between experimental and calculated values of Γ_c. The published background thermal conductivity has a value of about 44 $mW \cdot m^{-1} \cdot K^{-1}$ in this region. Of this, the dilute gas term in (1)

comprises about 14 $mW \cdot m^{-1} \cdot K^{-1}$. It has been calculated by Hanley and Ely [15] from theoretical considerations with an estimated uncertainty of 3%. The remaining 30 $mW \cdot m^{-1} \cdot K^{-1}$ was correlated by Hanley et al. [1] using the data of Ziebland and Burton [16]. This data set consists of 64 points covering the range 80–200 K, measured with a concentric cylinder apparatus. Of these only about one-fourth lie in the temperature range of interest here. The correlators have estimated the overall uncertainty of the correlated background values to be 4%. This appears to be about the standard deviation from the data of [16] and may not make sufficient allowance for any systematic errors. No measurements were made near the critical density, and thus the correlation is merely an interpolating function in this region. New measurements on λ^B for oxygen are now underway in our laboratory. Meanwhile, for the present purposes we will adjust the background values downward by 18%.

The damping function, $F(\Delta T^*, \Delta\rho^*)$, is completely empirical, and although its form is reasonable, our main justification for its use here is the fact that it has worked well for a number of other substances. The values for the parameters A and B given earlier were used by Hanley et al. [1] to represent the data for argon, krypton, xenon, nitrogen, and oxygen. Their claim, however, that those values are approximately universal is probably not correct. Basu and Sengers [5] have recently fit the best data for CO_2, allowing A and B to be adjustable parameters. Their values, $A = 39.8$, $B = 5.45$ give a somewhat better fit to our data and are therefore used here. Obviously there is a certain amount of correlation between the values of F and λ^B. Until the latter has been determined more accurately we cannot say more about F.

The other quantities to be examined are all part of the critical enchancement term in Eq. (16), and thus their behavior shows up most prominently in the data nearest T_c. We will consider only the critical isochore first. The viscosity has been measured by Haynes [17], with an estimated uncertainty of 2%. The critical enhancement, η/η_B, was taken from [6], where it reproduced high quality data for nitrogen to within $\pm 2\%$. The uncertainty in the value of q to be used for oxygen probably does not add more than an additional 1% uncertainty. The enhancement has a value of 1.03 at $\Delta T = 1$ K, increasing to 1.25 for the data nearest critical. The correlation length ξ is expected to be represented quite well by Eq. (8). The amplitude ξ_0, however, can only be calculated via Eq. (5) with an uncertainty of about 10%. An independent experimental determination of ξ_0 would be most useful. The value used for Λ, 1.2, allows relatively good agreement with the data. Any conclusions we may draw about its value from comparisons with our data, however, must taken into account the fact that it depends on the values chosen for ξ_0 and η, and it therefore should be

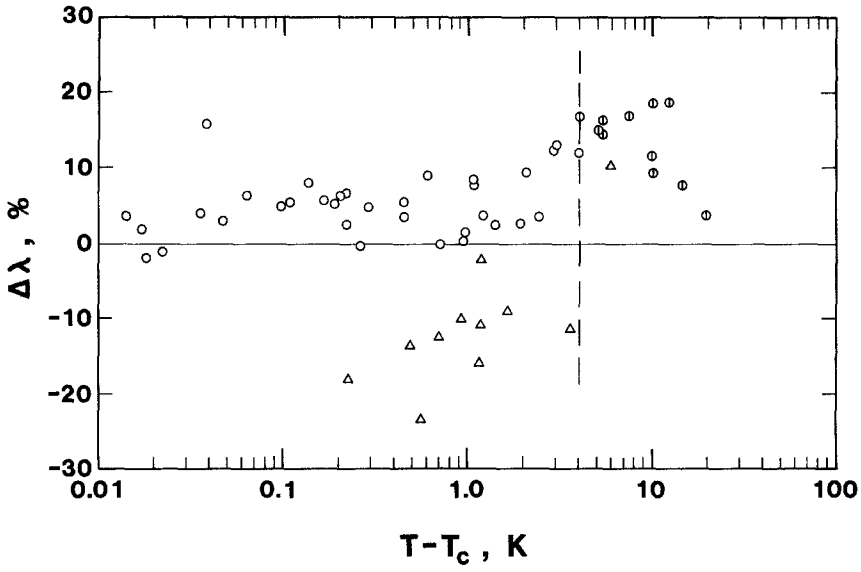

Fig. 5. Deviations between data and model: circles, circles with lines, critical isochore; triangles, 15.3 mol · liter^{-1} isochore; dashed line, limit of range of scaled equation.

assigned an uncertainty of ± 10%. Deviations between the calculated and experimental thermal conductivity on the critical isochore are shown in Fig. 5. There we see that on the average, the calculated values seem to be about 5% higher near T_c. Overall, however, the agreement is considered quite good. Further from critical, where the polynomial representation of the PVT surface is used, the agreement is also relatively good with maximum deviations being about 15% at $\Delta T = 5$ K.

Away from the critical isochore, the agreement is not so good. This situation may be due to the fact that the data appear to be of lower quality and, possibly, also to the fact that the PVT surface may be represented less accurately by the equation of state. In Fig. 5 the data on the 15.3 mol · liter^{-1} ($\Delta\rho^* = 1.12$) isochore deviate by up to 20%. Although the data scatter rather badly, there does seem to be a discernible systematic trend, which suggests that the deviations would become worse as the critical temperature is approached. A very similar behavior is seen in Fig. 6, which shows the deviations on the saturated vapor and liquid boundary. Here the deviations also reach 20%; 27% for one point at $T_c - T = 0.002$ K. Correction for the fact that the scaled equation of state does not reproduce well the directly measured compressibilities from [14] at the saturation boundary improves the agreement somewhat, but a large discrepancy remains. Assumption of a temperature gradient due to local heating by the laser beam would also improve the agreement for the saturated vapor data but would

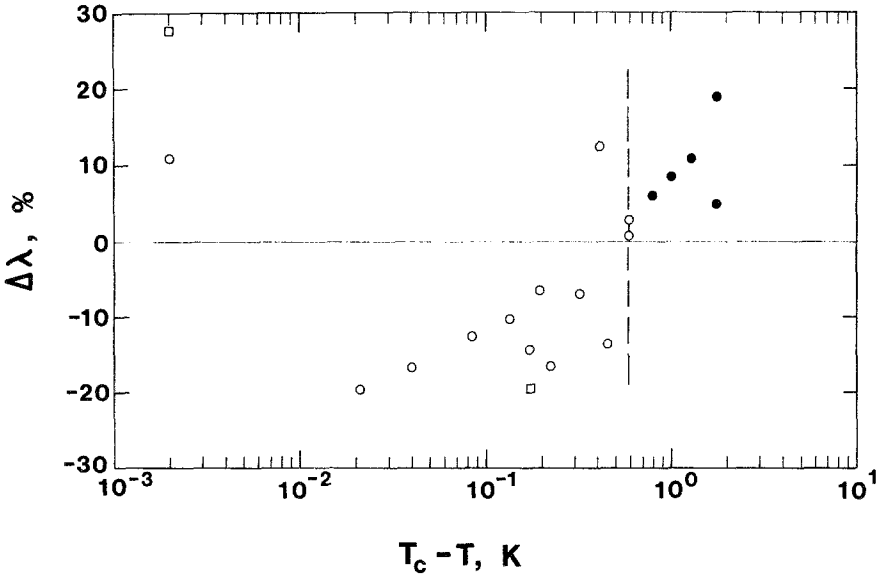

Fig. 6. Deviations for the saturated vapor ○, ●, and liquid □.

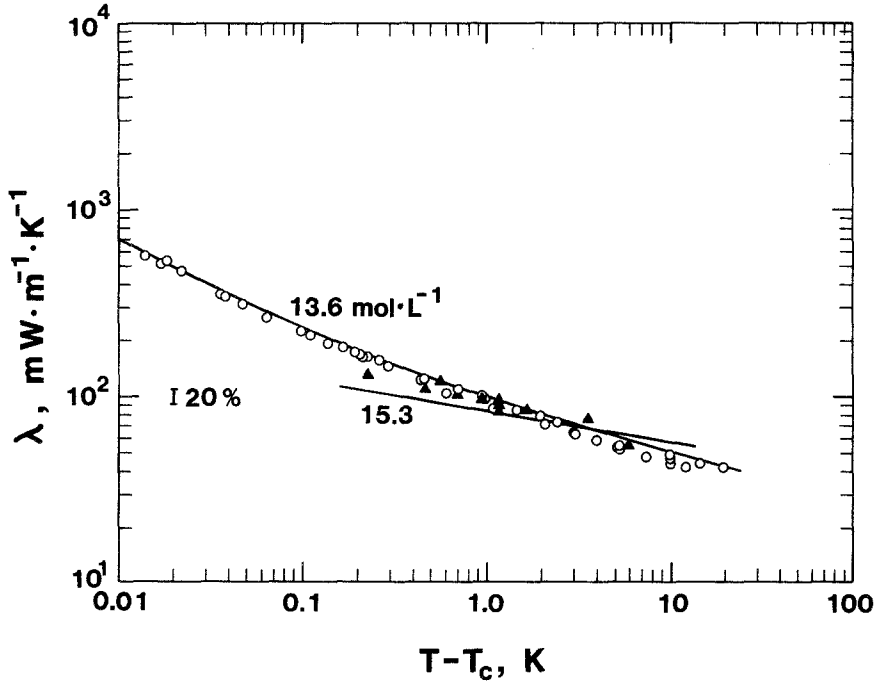

Fig. 7. The thermal conductivity from the data and model: ○, critical isochore; ▲, 15.3 mol · liter^{-1} isochore.

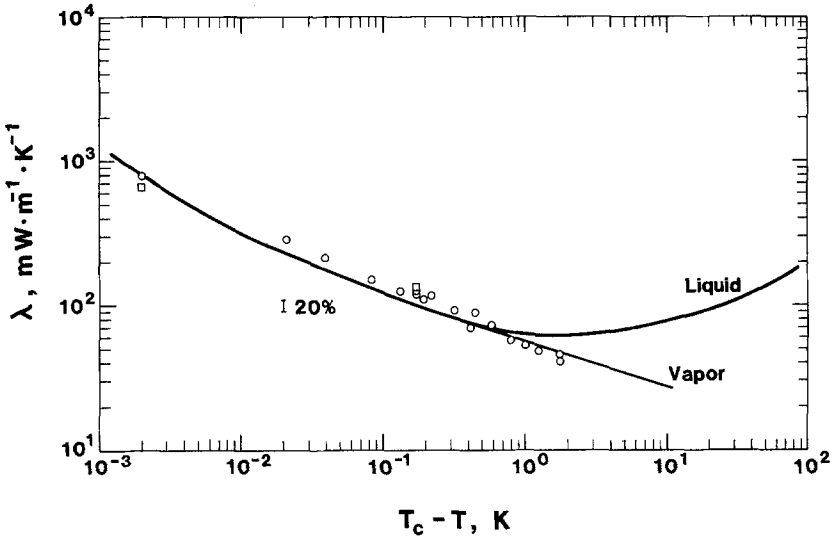

Fig. 8. Thermal conductivity from the data and model for the saturated vapor, ○, and liquid, □.

not significantly change the disagreement on the 15.3 mol · liter^{-1} isochore. Derived results for the thermal conductivity are compared with calculated values in Figs. 7 and 8.

6. SUMMARY

We have measured the thermal diffusivity of oxygen on the critical isochore, one other isochore, and the saturation boundary at temperatures varying from 0.002 to 20 K from T_c, by means of Rayleigh light scattering. The results were compared with theoretical model calculations based on the Stokes-Einstein equation as modified by Kawasaki and implemented by Sengers. The agreement is good at the critical density, but there are some fairly large, systematic differences at the other densities. Some possible explanations are offered for these differences, but it is not possible to decide from the present work whether the model is correct for oxygen in these regions. By making use of the appropriate equations of state, we have derived the thermal conductivity from the data.

REFERENCES

1. H. J. M. Hanley, R. D. McCarty, and W. M. Haynes, The viscosity and thermal conductivity coefficients for dense gaseous and liquid argon, krypton, xenon, nitrogen, and oxygen, *J. Phys. Chem. Ref. Data* 3(4):979 (1974).

2. L. P. Kadanoff and J. Swift, *Phys. Rev.* **166**:89 (1968).
3. K. Kawasaki, *Phys. Rev.* **150**:291 (1966).
4. J. V. Sengers and J. M. H. Levelt Sengers, Critical phenomena in classical fluids, in *Progress in Liquid Physics*, C. A. Croxton, ed. (John Wiley & Sons, Chichester, 1978), Chap. 4.
5. R. S. Basu and J. V. Sengers, Thermal conductivity of fluids in the critical region, 16th Int. Thermal Conductivity Conf., Chicago (1979).
6. R. S. Basu and J. V. Sengers, *J. Heat Transfer* **101**:3 (1979).
7. H. C. Burstyn, J. V. Sengers, and P. Esfandiari, *Phys. Rev. A* **22**:282 (1980).
8. L. A. Weber, A modified Benedict-Webb-Rubin equation of state for gaseous and liquid oxygen, Natl. Bur. Stand. (U.S.), Interagency Report NBSIR 78-882 (1978).
9. L. A. Weber, *J. Res. Natl. Bur. Stand.* (U.S.) **74A**:93 (1970).
10. J. V. Sengers, *Ber. Bunsenges. Physik. Chem.* **76**:234 (1972). Ibid, in *Transport Phenomena*-1973, J. Kestin, ed., AIP Conference Proceedings No. 11 (American Institute of Physics, New York, 1973), p. 229.
11. H. J. M. Hanley, J. V. Sengers, and J. F. Ely, On estimating thermal conductivity coefficients in the critical region of gases, in *Thermal Conductivity 14, Proc. 14th Int. Conf.*, Storrs, Conn., 1975, P. G. Klemens and T. K. Chu, eds. (Plenum Press, New York, 1976), p. 383.
12. B. J. Ackerson and G. C. Straty, *J. Chem. Phys.* **69**:1207 (1978).
13. H. M. Roder and L. A. Weber, *ASRDI Oxygen Technology Survey, Vol. I: Thermophysical Properties* (NASA SP-3071, 1972).
14. L. A. Weber, *Phys. Rev.* **A2**:2379 (1970).
15. H. J. M. Hanley and J. F. Ely, *J. Phys. Chem. Ref. Data* **2**(2):735 (1973).
16. H. Ziebland and J. T. A. Burton, *Br. J. Appl. Phys.* **6**:416 (1955).
17. W. M. Haynes, *Physica* **89A**:569 (1977).